DNA Binding and Aggregation Properties of the Vaccinia Virus I3L Gene Product

Article *in* Journal of Biological Chemistry · August 1999

DOI: 10.1074/jbc.274.31.21637 · Source: PubMed

4 authors:

Michael Tseng
University of Toronto
7 PUBLICATIONS **376** CITATIONS
SEE PROFILE

Nades Palaniyar
University of Toronto
194 PUBLICATIONS **6,200** CITATIONS
SEE PROFILE

Wandong Zhang
University of Ottawa
115 PUBLICATIONS **5,016** CITATIONS
SEE PROFILE

David H Evans
University of Alberta
108 PUBLICATIONS **3,935** CITATIONS
SEE PROFILE

THE JOURNAL OF BIOLOGICAL CHEMISTRY
Vol. 274, No. 31, Issue of July 30, pp. 21637–21644, 1999

Printed in U.S.A.

DNA Binding and Aggregation Properties of the Vaccinia Virus I3L Gene Product*

(Received for publication, November 30, 1998, and in revised form, April 14, 1999)

Michael Tseng, Nades Palaniyar, Wandong Zhang‡, and David H. Evans§

From the Department of Molecular Biology & Genetics, University of Guelph, Guelph, Ontario N1G 2W1, Canada

The vaccinia virus I3L gene encodes a single-stranded DNA-binding protein which may play a role in viral replication and genetic recombination. We have purified native and recombinant forms of gpI3L and characterized both the DNA-binding reaction and the structural properties of DNA-protein complexes. The purified proteins displayed anomalous electrophoretic properties in the presence of sodium dodecyl sulfate, behaving as if they were 4-kDa larger than the true mass. Agarose gel shift analysis was used to monitor the formation of complexes composed of single-stranded DNA plus gpI3L protein. These experiments detected two different DNA binding modes whose formation was dependent upon the protein density. The transition between the two binding modes occurred at a nucleotide to protein ratio of about 31 nucleotides per gpI3L monomer. S1 nuclease protection assay revealed that at saturating protein densities, each gpI3L monomer occludes 9.5 ± 2.5 nucleotides. In the presence of magnesium, gpI3L promoted the formation of large DNA aggregates from which double-stranded DNA was excluded. Electron microscopy showed that, in the absence of magnesium and at low protein densities, gpI3L forms beaded structures on DNA. At high protein density the complexes display a smoother and less compacted morphology. In the presence of magnesium the complexes contained long fibrous and tangled arrays. These results suggest that gpI3L can form octameric complexes on DNA much like those formed by *Escherichia coli* single-stranded DNA protein. Moreover, the capacity to aggregate DNA may provide an environment in which hybrid DNA formation could occur during DNA replication.

Poxviruses are large DNA viruses which replicate in the cytoplasm of infected cells. Viral replication depends upon a viral-encoded DNA polymerase and probably utilizes a "rolling hairpin" mechanism (reviewed in Ref. 1). This replication scheme is attractive, because it can account for the concatemeric intermediates formed in infected cells and the absence of a virus-encoded DNA primase. The displacement of single-stranded replicative intermediates also provide substrates for a simple recombination model in which recombinant molecules originate as hybrid duplexes formed through the annealing of complementary single-stranded DNA (ssDNA).[1] Such a scheme rationalizes the extraordinarily high frequency of genetic recombination seen in poxvirus-infected cells (2), the abundance of heteroduplex DNA formed at the onset of DNA replication (3), and the inextricable linkage between poxviral DNA replication and genetic recombination (4).

The single-stranded DNAs involved in these replication and recombination reactions do not exist in an uncomplexed state inside cells. Indeed, a number of new DNA-binding proteins are synthesized when the poxvirus vaccinia infects a cell. Some of these proteins are expressed late in the infective cycle and probably aid in the condensation and packaging of the double-stranded viral genome. However, a 34–35-kDa phosphoprotein with a high affinity for ssDNA is expressed early and at intermediate times post-infection and can be purified from vaccinia replication complexes (5–7). The protein was subsequently shown to form an association with the viral ribonucleotide reductase and to be encoded by the vaccinia virus I3L gene (8). These observations suggest that gpI3L is an important component of the poxviral replicative complex which binds to exposed ssDNA and may ensure that dATP synthesis, which might otherwise trigger apoptosis (9), is localized near sites of DNA replication. Research conducted in P. Traktman's laboratory (10) indicates that gpI3L is almost certainly an essential gene product and strongly supports the contention that it is a key component of the viral replication and/or repair machinery.

Whether gpI3L plays any role in promoting poxviral recombination is unknown. However, there exists abundant genetic and biochemical evidence showing that single-strand DNA-binding proteins (SSB) serve a key role in bacteriophage recombination. For example, the λ Red recombination pathway depends upon a phage-encoded 5′-3′ exonuclease, Redα, and a SSB called Redβ. Redβ protein not only promotes DNA renaturation *in vitro* (11), but also catalyzes strand transfer (12) by binding to the hybrid DNA which forms during strand annealing. This explains how the λ Red recombination pathway produces long hybrid joints *in vivo* in the absence of *Escherichia coli* RecA protein (13). Bacteriophage T7 SSB (gene 2.5) also catalyzes joint molecule formation and, in the presence of the gene 4 helicase, facilitates efficient polar DNA strand transfer (14). This again permits high-frequency T7 recombination even in *recA E. coli*. Much less is known about the SSBs encoded by mammalian viruses because such viruses are not so amenable to genetic analysis as are bacteriophage. However, biochemical studies have shown that the herpes simplex virus SSB (ICP8) can catalyze renaturation of complementary DNA strands and strand transfer *in vitro* (15, 16). Herpes simplex virus-1 catalyzes an efficient replication-dependent recombination reaction (17) and these biochemical properties suggest that ICP8 could catalyze step(s) in the viral recombination reaction.

* This work was supported by Medical Research Council of Canada Grant MT-10923 and by a grant in support of the University of Guelph Electron Microscopy Facility from the Natural Sciences and Engineering Research Council. The costs of publication of this article were defrayed in part by the payment of page charges. This article must therefore be hereby marked "*advertisement*" in accordance with 18 U.S.C. Section 1734 solely to indicate this fact.

‡ Ontario graduate scholar.

§ To whom correspondence should be addressed: Dept. of Molecular Biology and Genetics, University of Guelph, Guelph, Ontario, N1G 2W1, Canada. Tel.: 519-824-4120 (ext. 2575); Fax: 519-837-2075; E-mail: dhevans@uoguelph.ca.

[1] The abbreviations used are: ssDNA, single-strand DNA; SSB, ssDNA-binding protein; nt, nucleotide(s).

In this article we have examined the DNA binding and aggregation properties of native and recombinant vaccinia virus gpI3L. The binding properties of SSBs are of particular interest because these properties vary depending on solution conditions and may influence how SSBs function in DNA replication, recombination, and repair. For example, *E. coli* SSB exhibits three distinct DNA binding modes (with binding site sizes of 35 ± 2, 56 ± 3, and 65 ± 3 nucleotides per SSB tetramer) of which the $(SSB)_{35}$ binding mode is favored at high binding density (29). Electron microscopic analysis has further shown that interconversion between these binding modes alters the structure of each complex, with a "beaded" structure being seen at low SSB-to-DNA ratios (where the $(SSB)_{56}$ and/or the $(SSB)_{65}$ forms are favored) and a "smooth-contoured" complex (27) being seen under conditions favoring the $(SSB)_{35}$ binding mode (29). Similar trends in binding mode transitions have also been observed using *Saccharomyces cerevisiae* yRPA proteins.

Our studies with vaccinia single-strand DNA-binding protein show that one can form complexes composed of gpI3L and ssDNA which likewise exhibit different structures depending upon the binding conditions. These complexes range in structure from simple "beads on strings" to huge, complex, DNA-protein aggregates. Poxviruses are known to very efficiently replicate and recombine transfected DNAs via a pathway that generates great quantities of heteroduplex DNA (2, 3, 18). Our observations provide some insights into the macromolecular complexes which may constitute components of this pathway.

EXPERIMENTAL PROCEDURES

Strains and Plasmids—Vaccinia virus strain WR was obtained from the America Type Culture Collection and propagated on HeLa cells. *E. coli* strain DE142 (BL21 DE3 *recA* p*Lys*S) was constructed in this laboratory (19). *E. coli* strain HS-1 (JM103 *thy*$^-$) was obtained from Dr. H. Schellhorn (McMaster University).

Nucleic Acids—Single-stranded and double-stranded M13mp19 phage DNAs were purified as described previously (20) and ϕX174 purchased from New England Biolabs. ^{3}H-Labeled DNA was prepared by infecting 1 liter of *E. coli* strain HS-1 with M13mp19 phage in the presence of 1 mCi of [^{3}H]thymidine (ICN). The specific activity of the purified ssDNA was 4,900 cpm/nmol nucleotide assuming 1 A_{260} = 30 μg/ml. Double-strand DNA concentrations were calculated assuming 1 A_{260} = 50 μg/ml. Single-strand DNA cellulose was prepared by the method of Alberts and Herrick (21) and contained 0.2 mg of bound DNA per ml of cellulose.

Molecular Cloning—Two oligonucleotides (5′-CGCGGATCCATGAGTAAGGTAATC-3′ and 5′-CCGGAATTCACATTGAATATTGGC-3′), *Taq* DNA polymerase (Promega), and the polymerase chain reaction were used to clone the I3L open reading frame from vaccinia virus DNA. The 0.8-kilobase pair reaction products were then cloned into the *Bam*HI and *Eco*RI sites of pET21a (Novagen), transformed into *E. coli* strain HB101, and sequenced. A single amino acid substitution differentiated our cloned gene product (Ser^{157}) from that reported for vaccinia strain WR (Ala^{157}). No attempt was made to alter this putative sequence polymorphism because the vaccinia Ankara and Copenhagen strains, like our WR stock, also encode serine at this site. The resulting recombinant protein bears a 14-amino acid N-terminal antigenic tag and a 20-amino acid C-terminal extension designed to facilitate Ni-chelate affinity chromatography.

Protein Purification—The recombinant protein was expressed in 1 liter of pNP105-transformed DE142 cells grown with shaking at 37° C in rich broth supplemented with ampicillin (100 μg/ml), chloramphenicol (25 μg/ml), and thymine (50 μg/ml). When the OD_{590} equaled 0.7, protein expression was induced by adding isopropyl-β-D-thiogalactoside (0.5 mM). Rifampicin (50 μg/ml) was added 0.5 h later and the cells recovered by centrifugation at 9,000 × *g* for 10 min at 4° C 3 h after inducing protein expression. The cells were harvested in 40 ml of binding buffer (0.5 M NaCl, 20 mM Tris·HCl, 60 mM imidazole·HCl (pH 7.9), 0.1 mM phenylmethylsulfonyl fluoride), and stored at −80° C.

The cells were thawed in a water bath and broken with 15 strokes of a tight-fitting Dounce homogenizer on ice. From this point all manipulations were performed at 0–4° C unless otherwise noted. The extract was centrifuged at 39,000 × *g* for 20 min (Fraction I, 490 mg of protein). Fraction I was applied to a 10-ml column of His-bind resin (Novagen), washed with 60 mM imidazole·HCl (pH 7.9) in wash buffer (0.5 M NaCl, 20 mM Tris·HCl (pH 7.9)), and eluted with a 20 ml of 0.06–1.0 M imidazole gradient in wash buffer. Protein-containing fractions were pooled to give Fraction II (6 mg of protein). Fraction II was immediately desalted into Buffer A (20 mM Tris·HCl (pH 7.8), 0.1 mM EDTA, 10 mM 2-mercaptoethanol, 10% (w/v) glycerol) containing 50 mM NaCl using a Bio-Gel 6-DG desalting column (Bio-Rad). Fraction II was applied to a 5-ml HiTRAP heparin column (Pharmacia), washed, and then eluted with a 0.06–2 M NaCl gradient in Buffer A. Protein-containing fractions were pooled, and then stored frozen at −80° C in small aliquots. The yield was 3.2 mg of protein/liter of culture at a final concentration of 2.6 mg/ml.

Native gpI3L was purified from vaccinia virus-infected HeLa cells using a procedure described by Rochester and Traktman (10) except that hydroxyurea was not added to infected cell cultures. Briefly, 18 g of virus-infected cells (1.2×10^{11} plaque-forming units, 6×10^9 cells) were harvested by centrifugation and broken by hypotonic shock and Dounce homogenization. The nuclei-free extract were applied to a 25-ml column of DEAE cellulose (Whatman) equilibrated with "DEAE buffer" containing 50 mM Tris·HCl (pH 7.4), 1 mM dithiothreitol, 1 mM EDTA, 10% (v/v) glycerol, and 50 mM NaCl. The flow-through was recovered, applied to a 25-ml column of single-stranded DNA cellulose equilibrated with DEAE buffer, and eluted with a 0.05–2.5 M NaCl gradient in DEAE buffer. The purest fractions eluted between 1.4 and 2.5 M NaCl as judged by gel electrophoresis. These fractions were pooled, dialyzed against Buffer A with 50 mM NaCl, concentrated with Sephadex G-50 powder, and stored frozen in small aliquots. This yielded 0.19 mg of native gpI3L protein at a final concentration of 100 μg/ml.

Protein Electrophoresis—Protein purity and molecular weights were determined using sodium dodecyl sulfate (SDS)-polyacrylamide gel electrophoresis. The proteins were visualized with a silver stain (Bio-Rad). Protein concentrations were determined using a commercial assay (Bio-Rad) and a bovine serum albumin standard. Molar concentrations were calculated assuming molecular masses of 30.0 and 33.5 kDa for the native and recombinant proteins, respectively.

Gel Shift, Aggregation, and Renaturation Assays—DNA-protein complexes were prepared for gel shift analysis by incubating 0–1.8 μg of protein with M13mp19 viral DNA in a 50-μl reaction containing 240 ng (0.1 pmol) of DNA, 12 mM Tris·HCl (pH 8.0), 2.5 mM 2-mercaptoethanol, 1 mM EDTA, and 12% (w/v) glycerol. After 20 min at 37° C, 4 μl of 6 times concentrated loading buffer (0.4 g/ml sucrose, 1.3 mg/ml bromphenol blue, 0.1 M EDTA) was added, and the DNA-protein complexes fractionated by gel electrophoresis. The gels were composed of 0.5% Seakem LE agarose and were run at 2 V/cm using a pH 8.0 buffer containing 89 mM Tris (or imidazole), 89 mM boric acid, and 2 mM EDTA. DNA was visualized by ethidium bromide staining and photographed.

The aggregation assays contained 0–1.5 μg of protein, 750 ng of single-stranded M13mp19 DNA, 33 mM Tris·HCl (pH 8.3), 1.8 mM dithiothreitol, 1 mM EDTA, and 5% (w/v) glycerol in a total volume of 30 μl. Double-stranded M13mp19 DNA (1.5 μg) and 20 mM $MgCl_2$ were also added where indicated. The reactions were incubated at 37 °C for 20 min and then centrifuged at 16,000 × *g* for 20 min at 4 °C. The DNA distribution in the pellet and supernatant were calculated as described by Heyer *et al.* (22) monitoring either a ^{3}H label in the ssDNA (Fig. 5) or using densitometry to quantitate the amount of single- and double-stranded DNA in ethidium-stained agarose gels (Fig. 6). In both cases a correction was applied to account for the small volume of DNA carried over from the supernatant into pelleted fractions.

S1 Nuclease Protection Assays—S1 protection assays measured the capacity of bound protein to protect ssDNA from digestion by S1 nuclease (22). ^{3}H-Labeled M13mp19 viral DNA (0.1 pmol) was incubated for 20 min at 37 °C in a 30-μl reaction containing 10 mM Tris·HCl (pH 8.0), 1 mM EDTA, and protein as indicated. The reaction volume was then adjusted to 0.1 ml with 50 μl of S1 salts (0.68 M NaCl, 80 mM potassium acetate (pH 4.6), 2.8 mM $ZnSO_4$, 14% (w/v) glycerol), 2 units of S1 nuclease, and water. The reactions were incubated at 37 °C for 30 min and the acid-precipitable radioactivity determined as described (23).

Electron Microscopy—DNA-protein complexes were fixed with 0.6% glutaraldehyde at room temperature for 10 min and then 10 μl applied to a colloidion-coated 400-mesh nickel grid. Twenty minutes later the grids were blotted dry with filter paper. The complexes were then stained for 30 s in 50 μM uranyl acetate in 90% (v/v) ethanol, washed for 10 s in 95% ethanol, and air dried. A 20-Å platinum shadow was applied at an angle of 22 °C, using a Balzers 360M evaporator, and the samples were imaged using a JEOL 100CX transmission electron microscope. All size measurements were determined using images of the native

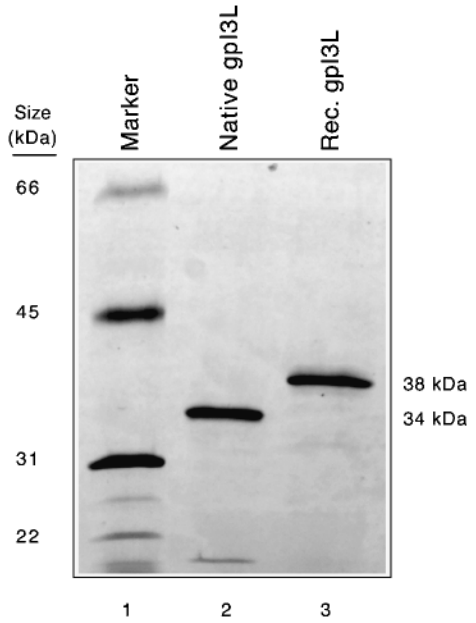

FIG. 1. **Gel electrophoretic analysis of gpI3L fractions.** A 20% SDS-polyacrylamide gel was prepared and 200 ng of either native or recombinant gpI3L applied to *lanes 2* and *3*, respectively. Protein was visualized by silver staining.

protein, a Hitachi KP-113 digital camera linked to a Power Macintosh 8600/200 computer, and NIH Image software. Print magnifications were calculated using a combination of microscope settings and photographic conversion factors.

RESULTS

Purification of Native and Recombinant gpI3L—Vaccinia virus gpI3L displays an unusually high affinity for ssDNA. This behavior was used to purify the native protein from virus-infected cells following the method of Rochester and Traktman (10). The resulting protein was 87–95% pure (depending upon the preparation) and these purity estimates were factored into all subsequent calculations of the protein's molar concentration (Fig. 1). Recombinant gpI3L was produced in *E. coli* as a histidine-tagged fusion protein and purified using a combination of Ni-chelate and heparin-affinity chromatography plus gel-exclusion chromatography. This protein preparation appeared pure by SDS-polyacrylamide gel electrophoretic analysis (Fig. 1). A comparison of the polypeptides produced by digesting each protein with trypsin confirmed the identity of the native protein (data not shown). Both forms of protein migrated unusually slowly on SDS-polyacrylamide gels. The predicted masses were 30.0 and 33.5 kDa for native and recombinant proteins, respectively, whereas we measured 34 and 38 kDa, respectively. Further investigations determined a mass of 33,596 Da for the recombinant protein by electrospray mass spectroscopy. This value is nearly identical to the 33,531 Da predicted for an *N*-formylated histidine-tagged protein and shows that reduced electrophoretic mobility in the presence of SDS is an intrinsic feature of gpI3L.

Gel Shift Analysis—Gel shift analysis was used to determine appropriate DNA binding conditions. Single-stranded ϕX174 DNA was incubated with varying quantities of recombinant gpI3L in a low ionic strength buffer containing Tris buffer, 2-mercaptoethanol, EDTA, and glycerol. The resulting complexes were then fractionated using agarose gel electrophoresis. It was noted that as the protein-to-DNA ratio was increased, the relative migration of the DNA decreased (Fig. 2). At the highest ratios of protein-to-DNA attainable in these reactions (~10 nucleotide per gpI3L monomer) the mobility was retarded approximately 50% compared with free DNA.

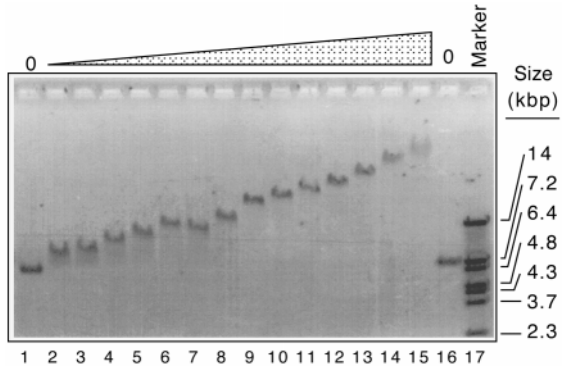

FIG. 2. **gpI3L binding to ϕX174 DNA assayed by electrophoretic mobility gel shift analysis.** Reactions contained 0.25 μg of single-stranded ϕX174 DNA and 0–5.1 μg of recombinant gpI3L. The DNA-protein complexes were fractionated by electrophoresis through a 0.5% agarose gel, stained with ethidium bromide, and visualized using ultraviolet light.

We also calculated the relative mobility of these complexes using the formula,

$$R_f = \frac{\text{Distance migrated}_{\text{DNA protein complex}}}{\text{Distance migrated}_{\text{uncomplexed DNA}}} \quad \text{(Eq. 1)}$$

and plotted these values *versus* the DNA-protein ratio. An interesting feature of these plots was a discontinuity in the retardation curves. This discontinuity occurred when the DNA to protein ratio equaled about 32 nucleotides per gpI3L monomer as judged by linear-regression analysis (Fig. 3, *panel A*). Beyond this "breakpoint" greater quantities of protein caused a disproportionately greater retardation of the DNA-protein complexes. We repeated the experiment using a larger M13mp19 DNA substrate and recombinant gpI3L so that the total mass of the complex would increase for a given nucleotide-to-protein ratio. The same discontinuity was still seen at about 30 nucleotides per monomer (Fig. 3, *panel B*). We concluded that at high protein densities (>1 monomer per ~31 nucleotides), gpI3L binds ssDNA differently than at low protein densities.

S1 Analysis—The blurring and fading of the DNA complexes which occurred at very high protein-DNA ratios (Fig. 2) complicated efforts to identify the point at which protein binding saturates. To better determine this saturation point we performed a quantitative investigation of gpI3L's DNA binding capacity using S1 protection analysis. The assay measured the degree to which bound protein protects ssDNA from S1 nuclease digestion. Varying quantities of recombinant gpI3L were incubated with a fixed amount of ^{3}H-labeled M13mp19 viral DNA, and then treated with an excess of S1 nuclease in S1 buffer. $MgCl_2$ was deliberately omitted from the binding reactions to minimize the interference which might result from aggregate formation (see below). The degree of S1 protection was then calculated from the amount of acid-precipitable radioactivity. These experiments showed that 100% S1 resistance was achieved when the DNA-protein ratio was about 9.5 nucleotides per gpI3L monomer (Fig. 4). Lower and upper 95% confidence intervals were 7.1 and 12.7 nucleotides per monomer, respectively.

Aggregate Formation—Besides binding DNA, gpI3L can also aggregate DNA, although the process required somewhat different reaction conditions. Aggregation can be demonstrated using a simple sedimentation assay. Reactions were prepared containing recombinant gpI3L and single-stranded M13mp19 DNA at protein-to-DNA ratios of up to 1 mol of protein per 50 mol of nucleotide. No aggregation was noted in the absence of $MgCl_2$, but in the presence of 20 mM $MgCl_2$ gpI3L catalyzed the formation of high molecular weight aggregates which sedi-

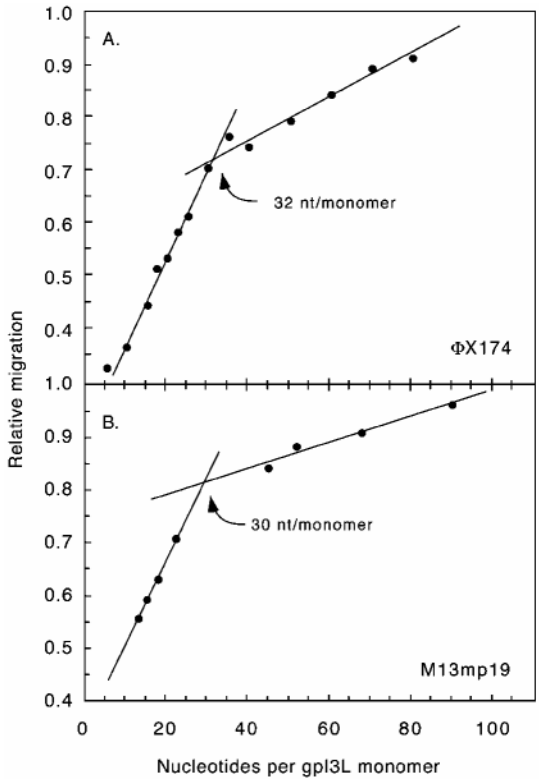

FIG. 3. **Effect of gpI3L concentration on electrophoretic mobility.** *Panel A*, the distance migrated by each of the DNA-protein complexes shown in Fig. 2 was determined along with that of free ϕX174 DNA and the ratio of the two values (R_f) plotted *versus* the mole ratio of nucleotides to protein. A break in the curve appears when the protein density equals 32 nt/monomer. *Panel B,* the experiment in *panel A* was repeated using single-stranded M13mp19 DNA. A similar break occurred at about 30 nt/monomer.

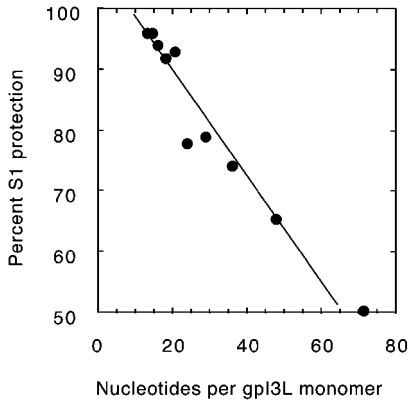

FIG. 4. **S1 protection assay.** ^{3}H-Labeled M13mp19 DNA was preincubated with the indicated quantities of recombinant gpI3L and then digested with a calibrated excess of S1 nuclease. The degree of S1 protection was determined by measuring the amount of acid-insoluble radioactivity. A least squares linear regression indicated that 100% protection required one gpI3L monomer per 9.5 nucleotides.

mented to the bottom of a microcentrifuge tube in 20 min at 16,000 $\times$ *g* (Fig. 5). To test whether this reaction was dependent upon properly folded gpI3L, we provided sufficient time for the complexes to form and then added 0.1% SDS. The detergent efficiently dissociated these rapidly sedimenting complexes.

The aggregation reaction promoted by gpI3L also showed a remarkable capacity to discriminate between double-stranded and ssDNAs. To test the binding specificity under these conditions, we prepared reactions containing $MgCl_2$, gpI3L, and an equimolar ratio of single- and double-stranded M13mp19 mol-

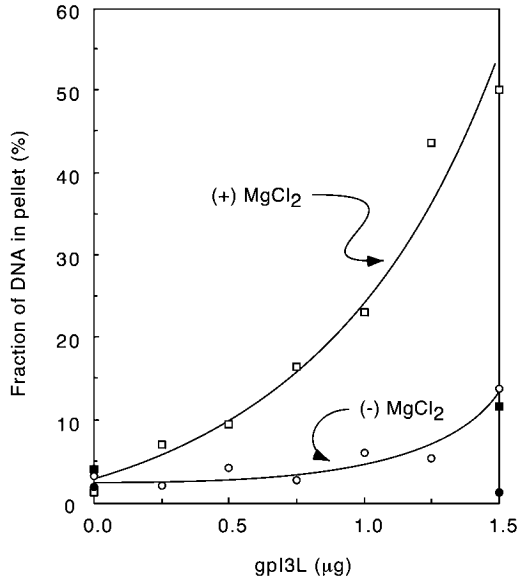

FIG. 5. **Aggregation of ssDNA by gpI3L in the presence of $MgCl_2$.** The indicated quantities of recombinant gpI3L were incubated with 1.5 μg of ^{3}H-labeled M13mp19 DNA in the presence (□) or absence (○) of 15 mM $MgCl_2$ and then centrifuged at 12,000 $\times$ *g* for 20 min at 4 °C. The distribution of radioactivity was then determined in the pellet and supernatant fractions by liquid scintillation counting. Adding SDS and proteinase K prior to the centrifugation step disrupted the rapidly sedimenting complexes (■, ●).

ecules. The protein-to-DNA ratios varied up to 1 mol of protein/40 mol of the nucleotide present in the single-stranded reaction component. When the pellet and supernatant fractions were examined by gel electrophoresis, after centrifugation, it was noted that only the ssDNA was precipitated by gpI3L (Fig. 6). The supernatant retained essentially all of the double-stranded molecules. Thus gpI3L interacts in a highly-specific manner with ssDNA under these binding conditions.

DNA Binding and Aggregation Properties of Native gpI3L—All of the experiments outlined above were repeated using native gpI3L (except for the S1 protection assay for which insufficient quantities of highly concentrated protein were available). The only clear and consistent difference between the two proteins was noted when gel shift assays were used to monitor DNA binding in the absence of magnesium ions (Fig. 7). When we measured the migration properties of the DNA-protein complexes, both proteins produced a break in the retardation curves at 30–35 nt per monomer. However, at any given DNA-protein mole ratio, complexes containing the smaller and phosphorylated native isoform (10) always migrated faster than did those composed of recombinant protein. To gain further insights into the nature of the structures formed by the two types of protein at different DNA-protein ratios, we employed electron microscopy.

Electron Microscopy—Several control experiments were first performed to determine the image resolution and identify potential artifacts. When gpI3L was spread on parlodian grids in the absence of DNA, it typically formed elliptical structures with axial dimensions 11 $\times$ 14 $\pm$ 2 nm (Figs. 8*B* and 9*A*) while naked DNA was too thin to be visualized using this shadowing and staining procedure (data not shown). When buffer was applied to the grids it left variable numbers of electron-dense beads in each grid field, varying in diameter from 30 to 60 nm (Fig. 8*A*). This buffer property shows that not all beads, particularly the larger ones, are necessarily composed of protein and suggested that the structures of DNA-protein complexes must be interpreted with caution.

When gpI3L was incubated with single-stranded ϕX174

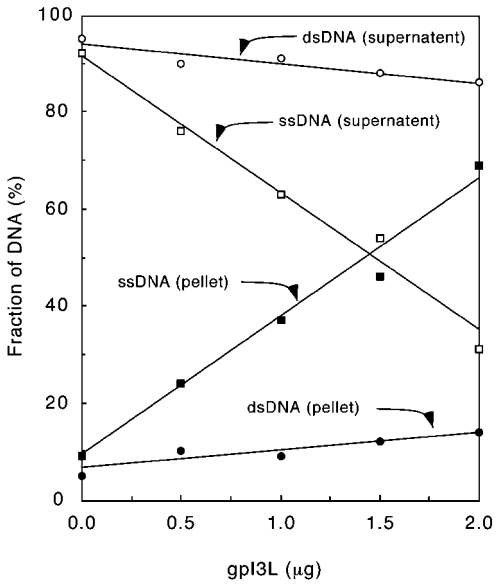

FIG. 6. **Selective aggregation of ssDNA in the presence of double-stranded DNA.** Reactions were prepared that contained the indicated quantities of recombinant gpI3L, 20 mM $MgCl_2$, and 1.5 μg of single-stranded plus 0.75 μg of double-stranded M13mp19 DNA. After incubation at 37 °C for 20 min, the samples were centrifuged for 20 min at 12,000 $\times$ *g* at 4 °C. The DNA distribution was determined in the pellet and supernatant fractions using agarose gel electrophoresis and densitometry.

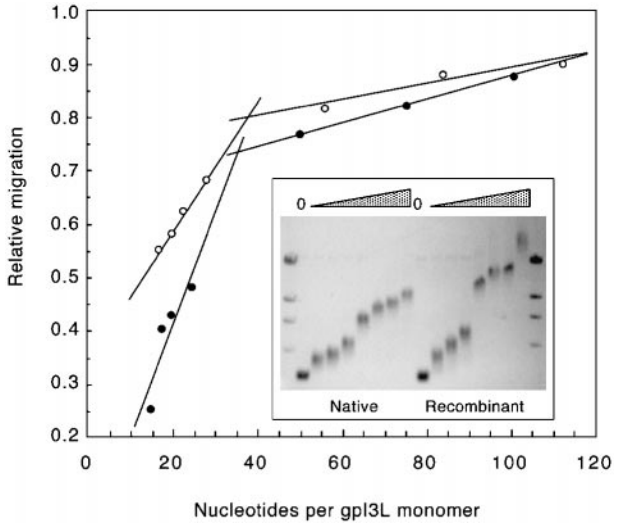

FIG. 7. **Electrophoretic behavior of complexes containing native or recombinant gpI3L.** Complexes were prepared containing the indicated quantities of native or recombinant gpI3L and the relative mobility determined as described (see Figs. 2 and 3).

DNA at a nucleotide-to-protein ratio of 20:1 and in the absence of magnesium, the DNA was easily visualized (Figs. 8*C*, 9*B*, and 9*D*). The DNA appeared to be thinly coated with small spheres not significantly different in dimension from those formed by protein alone (13 $\times$ 17 $\pm$ 2 nm) which we will refer to as "15-nm" particles or beads. These DNA-protein complexes seemed to comprise continuous circles although twisted and/or linear complexes were also seen. However, the DNA path could not be followed continuously with certainty, because it often disappeared where clusters of smaller spheres formed slightly larger beaded structures 17 $\times$ 21 $\pm$ 2 nm in diameter ("20 nm" particles). We estimated that the DNA-protein complexes contained over 30 15-nm particles per circle although this should be considered only a rough estimate due to the difficulty of determining the number of 15-nm particles clumped within the

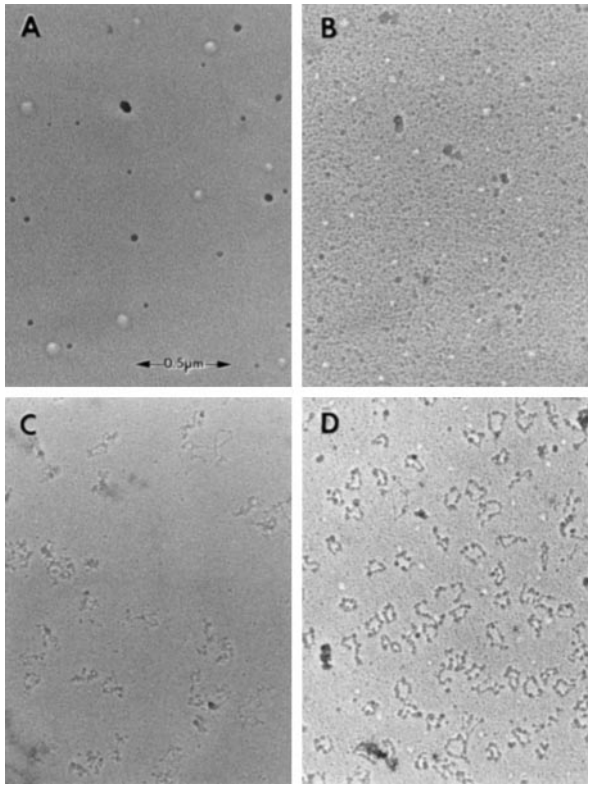

FIG. 8. **Electron microscopic analysis of gpI3L-DNA interactions.** *Panel A,* reaction buffer containing $MgCl_2$. *Panel B*, recombinant gpI3L alone. *Panel C,* recombinant gpI3L plus single-stranded ϕX174 DNA at a nucleotide to protein ratio of 20:1, no $MgCl_2$. *Panel D,* the same reaction as shown in *panel C*, but at a nucleotide to protein ratio of 40:1. All electron micrographs were imaged and printed using the same scale (as seen in *panel A*).

larger beads. The overall path length was measured using the best resolved and most extended molecules and found to be 600 $\pm$ 40 nm. Although the invisibility of protein-free ϕX174 DNA under these spreading conditions precluded a direct measurement of its path length, 5400 nt of ssDNA would extend 1.7–1.9 μm assuming an average residue spacing of 0.32–0.35 nm (24). Therefore gpI3L compacts DNA 2.6–3.4-fold at these DNA-protein ratios. There was no consistent difference in the appearance of molecules containing native or recombinant gpI3L even though the complexes were formed under conditions which produced different degrees of electrophoretic retardation on agarose gels.

These experiments were repeated using a nucleotide-to-protein ratio of 40:1, to gain some insights into the structural transition which is responsible for the break in the electrophoretic migration at ~31 nt/monomer. Interestingly, when the DNA was spread under these conditions the extended 15 nm-thick filaments, which form at a 20:1 nucleotide to protein ratio, were not seen. Instead, the majority of the molecules took on a uniform appearance consisting of condensed DNA circles composed entirely of 20-nm beads (18 $\times$ 23 $\pm$ 3 nm) with approximately 15 beads per circle (Figs. 8*D*, 9*C*, and 9*E*). The path length was 320 $\pm$ 30 nm suggesting that the DNA was significantly more compacted than was seen using greater quantities of gpI3L. The compaction was 4.8–6.5-fold relative to the theoretical length of naked DNA. Again there were no obvious structural differences between complexes composed of native *versus* recombinant gpI3L.

Quite different structures were formed when native and recombinant gpI3L were incubated with single-stranded ϕX174 DNA in the presence of 15 mM $MgCl_2$ prior to spreading

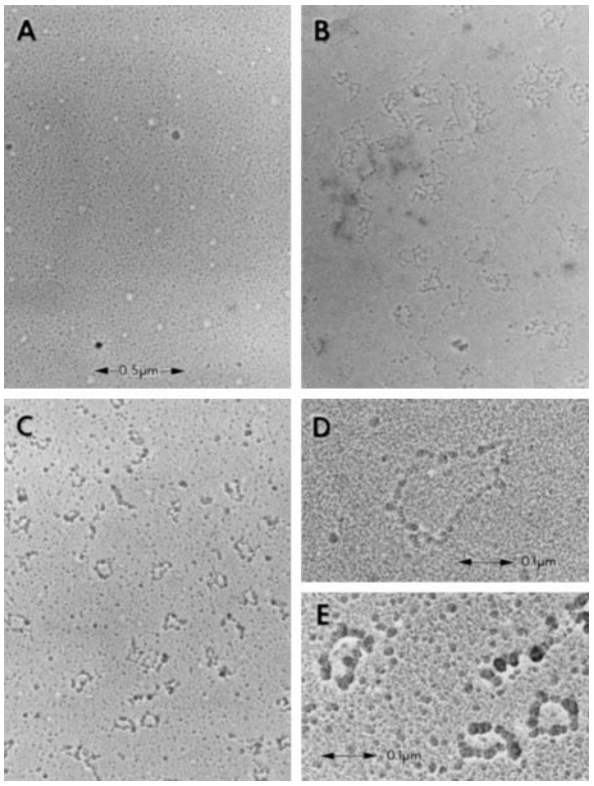

FIG. 9. **Electron microscopic analysis of gpI3L-DNA interactions.** *Panel A,* native gpI3L alone. *Panel B*, native gpI3L plus single-stranded ϕX174 DNA at a nucleotide to protein ratio of 20:1, no $MgCl_2$. *Panel C,* the same reaction as shown in *Panel C*, but at a nucleotide to protein ratio of 40:1. *Panel D*, higher resolution image of a molecule seen in *panel B*. *Panel E,* higher resolution image of a molecule seen in *panel C*. *Panels A-C* were imaged and printed using the same scale as shown in *panel A*. *Panels D* and *E* are 3.3 × photographic enlargements of particular molecules.

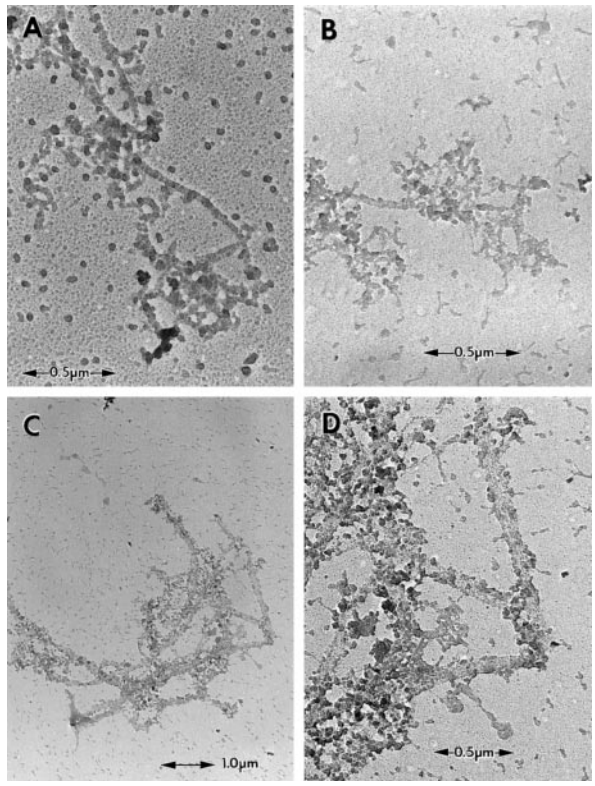

FIG. 10. **Electron microscopic analysis of gpI3L-DNA interactions in the presence of $MgCl_2$.** All reactions contained gpI3L plus single-stranded ϕX174 DNA at a nucleotide to protein ratio of 40:1 and 13 mM $MgCl_2$. *Panel A,* recombinant gpI3L. *Panel B,* native gpI3L. *Panel C,* native gpI3L. *Panel D,* higher resolution image of the molecule seen in *panel C*. Note the thick filaments.

(Fig. 10). Although some individual complexes were still formed under these conditions, much of the DNA and protein formed very large aggregates in which it was impossible to delineate the individual macromolecular components. In places thick filaments were visible sometimes singly or, more commonly, lying side by side. Single filaments were 22 ± 2 nm wide (Fig. 10*B*), while the side by side complexes varied in width. The best resolved of these side by side complexes were 125 ± 20 nm wide and appeared to be composed of 4 or 5 thick filaments (Fig. 10, *C* and *D*). Both native and recombinant gpI3L formed these aggregates, but again no obvious differences in the appearance of molecules containing either protein could be detected at this resolution. There was also no obvious differences in the appearance of aggregates formed using 20:1 or 40:1 nucleotide to protein ratios (data not shown).

DISCUSSION

Our data support and extend work previously reported by Davis and Mathews (8) and Rochester and Traktman (10). These earlier data showed that the vaccinia virus I3L gene encodes a high affinity ssDNA-binding protein. Native and recombinant proteins migrated anomolously slowly during SDS-polyacrylamide gel electrophoresis (Fig. 1). Both behaved like proteins that are 4 kDa larger than their actual size while mass spectroscopy showed that the recombinant protein does exhibit the expected mass. Although neither of the earlier publications commented specifically on this discrepancy, inspection of the data presented in these papers confirmed that this is a *bona fide* property of gpI3L. The origin of this phenomenon is unclear as gpI3L bears no great excess of proline and/or glycine residues and the pI is predicted to be 5.7. The protein does encode a very high proportion of polar residues (95 out of 269 residues in native gpI3L) which might account for this electrophoretic behavior. Whatever the cause of this anomaly, it suggests that like gpH5R (25) the identity and masses of vaccinia virus DNA-binding proteins needs to be interpreted with care.

Gel shift experiments detected evidence of two DNA binding modes. When the nucleotide to protein ratio was 31 or greater, increasing the amount of gpI3L relative to the number of nucleotides slowly reduced the electrophoretic mobility of the DNA-protein complexes (Fig. 2). Protein appeared to be distributed equally across all of the molecules confirming the low cooperativity of binding previously noted by Rochester and Traktman (10). A breakpoint in the retardation curves appeared at about 31 nt/monomer and thereafter greater quantities of protein resulted in a more dramatic reduction in the electrophoretic mobility. The same phenomena was seen using ϕX174 (5400 nt) and M13mp19 (7250 nt) DNAs. The fact that nearly identical DNA-to-protein ratios were calculated for the break point, using differently sized DNA-protein complexes, suggested that the effect was not caused by an electrophoretic artifact but rather by a structural transition which occurs when the DNA-protein ratio exceeds 31 nt/monomer.

Of course the accuracy of this value is dependent upon the assumption that most of the protein added to each binding reaction is active. This is difficult to prove when we have no enzymatic activity beyond DNA binding to monitor. However, we measured essentially identical DNA-protein stoichiometries at the breakpoints in the gel shift curves produced using either native or recombinant proteins. This suggested that most of the protein added to our reactions was active since it seems un-

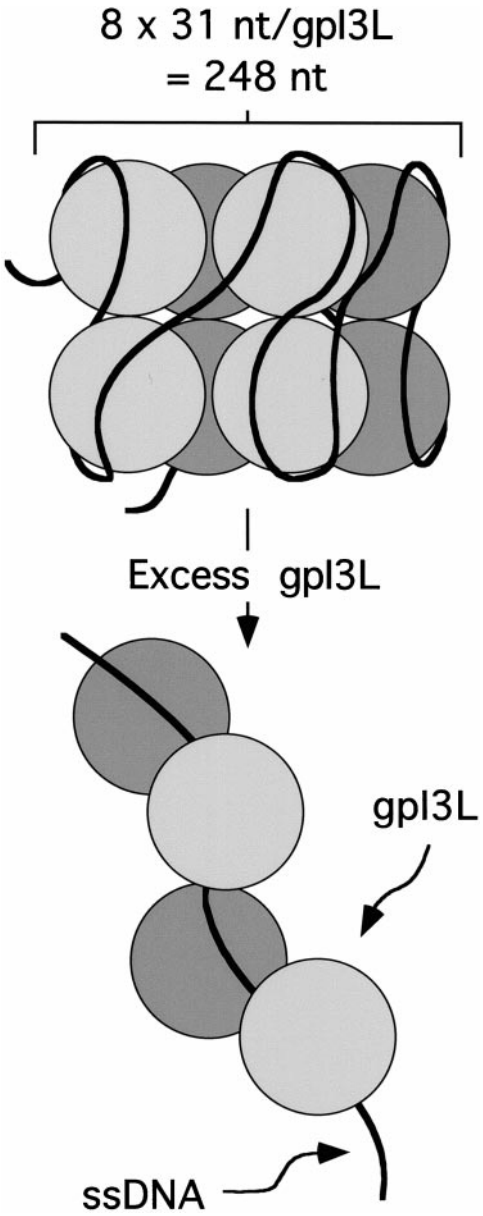

FIG. 11. **Hypothetical arrangement of DNA and protein in the 20-nm beads and 15-nm fibers.** We propose that the DNA folds upon an octamer of gpI3L at low protein densities. This would form the 20-nm beads and incorporate about 250 nt. Further addition of gpI3L would compete for DNA-binding sites in the linker regions, thus disrupting the octameric arrangement and generating 15-nm fibers. These fibers may consist of DNA bound to gpI3L dimers. This would be compatible with the calculated dimensions of a protein dimer (about 10 nm) if 5 nm of stain is subtracted from the measured fiber width (15 ± 2 nm).

likely that, if gpI3L is prone to inactivation during purification, two different protein preparations prepared by two very different methods would contain equally large quantities of inactive protein. In fact the only notable difference between the two forms of protein was that native complexes always migrated faster than did those composed of recombinant protein at any given DNA-protein mole ratio (Fig. 7). This behavior is to be expected given the greater molecular weight of the recombinant protein. Although we had hoped to gain some insights into why native gpI3L is phosphorylated through our work, more sophisticated studies are clearly needed to detect what may be quite subtle effects of DNA affinity or protein structure.

As discussed below, the simplest explanation for the appearance of breakpoints in the gel shift curves are that the structures formed on DNA at low protein densities are the more compact "beads on a string" form, while high densities of protein force the DNA to adopt a linear, more extended configuration. A corollary would be that under these low salt conditions, where essentially all of the protein is expected to bind and the components form electrophoretically stable complexes, one DNA binding mode becomes saturated when there is one molecule of protein per 31 nt of ssDNA. Similar results have been seen with *E. coli* SSB and *S. cerevisiae* yRPA proteins. At low protein densities "high site size" complexes of DNA and protein are formed consisting of beaded structures, while at high protein densities "low site size" complexes acquire a smooth appearance (26–28). As mentioned previously it has been noted that *E. coli* SSB binding modes are affected by other solution properties such as salt composition and pH (29). We expect that by investigating how these parameters affect gpI3L binding, we can determine how closely gpI3L resembles *E. coli* SSB.

Studies using oligonucleotides and quantized electrophoretic mobility shift assays do not detect a binding site spanning 31 nt, rather they show that each monomer of gpI3L can bind about 10 nt of DNA (10). We re-investigated this issue using a traditional S1 nuclease protection assay and discovered that at very high protein densities, complete S1 protection is achieved at 9.5 ± 2.5 nt/protein monomer (Fig. 4). The close congruence between oligonucleotide binding and S1 protection analyses suggests that a second binding mode indeed saturates at about 10 nt per monomer. Moreover, the fact that these nucleotides are protected from endonucleolytic attack suggests that this binding involves a close, high affinity interaction between DNA and protein. Presumably the DNA is occupying a binding site which functionally resembles the 8–10-nucleotide long DNA binding cleft of human RPA70 (30).

Somewhat different results were obtained when DNA-protein complexes were assembled in the presence of magnesium. Under these conditions high molecular weight aggregates formed which were sufficiently large to sediment in a microcentrifuge and unable to enter agarose gels. Double-stranded DNA was effectively excluded from the aggregates as one might expect given gpI3L's low affinity for double-strand DNA (8, 10). A particularly interesting feature of such aggregates is that they can potentially provide an environment which favors DNA annealing reactions, but whether these aggregates provide a suitable venue for such reactions remains uncertain at this time. Preliminary experiments suggest that annealing does occur under aggregation conditions in the presence of magnesium[2]; however, the reaction is most efficiently catalyzed by the recombinant protein for reasons which remain unclear at present.

Electron microscopy provides considerable insights into the structures responsible for the reactions outlined above. When imaged in the absence of DNA, native gpI3L showed a nearly spherical appearance, forming structures whose axial dimensions were 11 × 14 ± 2 nm. This measurement included some thickness contributed by the platinum shadow and uranyl acetate stain. Since these metals typically contribute 4–6 nm of additional width,[3] the true axial dimensions of gpI3L under these conditions are 6 × 9 nm with an estimated error of 2–3 nm in either dimension. Given that a 30-kDa spherical protein has a calculated diameter of about 5 nm (if the density is assumed to be 0.75 g/ml), then these measurements are in reasonable agreement with the fact that gpI3L behaves as a monomer in solution (10).

[2] M. Tseng and D. H. Evans, unpublished observations.
[3] G. Harauz, personal communication.

When gpI3L was spread with ssDNA in the absence of magnesium, two different types of structures were seen depending upon the protein density. At lower protein concentrations (40 nt/protein monomer) the DNA took on a beaded appearance reminiscent of the nucleosome-like structures formed by *E. coli* single-strand DNA-binding protein (26). There were 15 ± 3 beads per circle with each bead showing axial dimensions of 18 × 23 ± 3 nm. If one assumes that all of the gpI3L is bound by fixation under these low salt conditions, then there must have been 5400/40 ≅ 135 molecules of gpI3L per ϕX174 circle and thus each 20-nm bead contained 135/15 = 9 ± 2 molecules of gpI3L. Some care must be taken not to overinterpret electron micrographs, since counting 20-nm beads is a very subjective exercise and we cannot be certain that all of the added protein is bound to DNA. However, it is a striking coincidence that the nucleosome-like beads which are formed by *E. coli* SSB each contain 8 protein monomers (see Ref. 26, reviewed in Ref. 31), a value well within the estimated error in our determination. Moreover, if each of these beads were to incorporate 8 × 31 = 248 nt into 20 nm and assuming that 248 nt would normally span about 80 nm (248 nt × 0.34 nm/nt), we could achieve an optimal packing ratio of about four. This is close to the 4.8–6.5-fold packing ratio seen at slightly less than saturating protein concentrations. Rochester and Traktman (10) have previously noted the conservation of key amino acid residues between gpI3L and *E. coli* SSB. Our data suggests that vaccinia gpI3L can also form octameric complexes in the presence of ssDNA much like its *E. coli* counterpart (Fig. 11).

Different structures were formed when the density of gpI3L was increased to 20 nt/protein monomer. The molecules took on a more heterogeneous appearance containing both 20-nm beads and 15-nm thick fibers. This structural transition is compatible with the gel shift data (Fig. 2) because as the 15-nm filaments formed on DNA, they would have a more substantial effect upon electrophoretic mobility than would the beaded structures. The excess protein could simply compete for binding to "linker" DNA and thus disassemble the 20-nm beads. Precisely how the protein is arranged on the DNA under these conditions cannot be deduced from our experiments although the thickness of the fibers formed at high protein densities (Fig. 9*D*) is most compatible with a monomeric/dimeric coating arrangement (Fig. 11). Again it is quite striking that, as is the case with *E. coli* SSB (27), the smooth complexes which form at high gpI3L densities are less compacted (2.6–3.4-fold) than are the beaded complexes formed at lower protein density (4.8–6.5-fold).

The addition of magnesium and gpI3L aggregated the DNA into large branched filamentous structures. In this respect gpI3L behaves very differently from *E. coli* SSB (29) and *S. cerevisiae* yRPA (28) where adding magnesium does not produce large DNA-protein aggregates. Instead, identical concentrations of magnesium to the one used here, alters the binding mode of *E. coli* SSB and compacts the DNA-protein complexes. Well resolved circular complexes are also formed by yRPA in the presence of $MgCl_2$. The appearance and dimensions of the gpI3L-containing filaments suggests that they might be composed of 20-nm beads aligned in parallel arrays. If so, it is tempting to speculate that at least some of the DNA might lie along the surface of these beads (Fig. 11) where it would be better positioned to bind bridging magnesium ions and thus form these arrays. Such an arrangement of DNA and protein might also facilitate the annealing of homologous sequences within DNA aggregates and minimally impede the movement of DNA polymerase as it copied a gpI3L-coated template. We expect that micrococcal nuclease footprinting will provide further insights into this intriguing issue.

Acknowledgments—We thank Dr. H. Schellhorn for providing bacterial strains, Dr. A. Hilliker for advice on statistics, Dr. G. Harauz and B. Harris for help with the electron microscopy, and Drs. J. Chen and G. Lajoie for performing the mass spectrometry.

REFERENCES

1. Traktman, P. (1990) *Curr. Top. Microbiol. Immunol.* **163,** 93–123
2. Evans, D. H., Stuart, D., and McFadden, G. (1988) *J. Virol.* **62,** 367–375
3. Fisher, C., Parks, R. J., Lauzon, M. L., and Evans, D. H. (1991) *Genetics* **129,** 7–18
4. Merchlinsky, M. (1989) *J. Virol.* **63,** 2030–2035
5. Polisky, B., and Kates, J. (1972) *Virology* **49,** 168–179
6. Sarov, I., and Joklik, W. K. (1973) *Virology* **52,** 223–233
7. Nowakowski, M., Bauer, W., and Kates, J. (1978) *Virology* **86,** 217–225
8. Davis, R. E., and Mathews, C. K. (1993) *Proc. Natl. Acad. Sci. U. S. A.* **90,** 745–749
9. Liu, X., Kim, C. N., Yang, J., Jemmerson, R., and Wang, X. (1996) *Cell* **86,** 147–157
10. Rochester, S. C., and Traktman, P. (1998) *J. Virol.* **72,** 2917–2926
11. Kmiec, E., and Holloman, W. K. (1981) *J. Biol. Chem.* **256,** 12636–12639
12. Li, Z., Karakousis, G., Chiu, S. K., Reddy, G., and Radding, C. M. (1998) *J. Mol. Biol.* **276,** 733–744
13. Stahl, M. M., Thomason, L., Poteete, A. R., Tarkowski, T., Kuzminov, A., and Stahl, F. W. (1997) *Genetics* **147,** 961–977
14. Kong, D., and Richardson, C. C. (1996) *EMBO J.* **15,** 2010–2019
15. Dutch, R. E., and Lehman, I. R. (1993) *J. Virol.* **67,** 6945–6949
16. Bortner, C., Hernandez, T. R., Lehman, I. R., and Griffith, J. (1993) *J. Mol. Biol.* **231,** 241–250
17. Dutch, R. E., Bianchi, V., and Lehman, I. R. (1995) *J. Virol.* **69,** 3084–3089
18. DeLange, A. M., and McFadden, G. (1986) *Proc. Natl. Acad. Sci. U. S. A.* **83,** 614–618
19. Zhang, W., and Evans, D. H. (1995) *Nucleic Acids Res.* **23,** 4620–4627
20. Zhang, W., and Evans, D. H. (1993) *J. Virol.* **67,** 204–212
21. Alberts, B., and Herrick, G. (1971) *Methods Enzymol.* **21,** 198–217
22. Heyer, W. D., Evans, D. H., and Kolodner, R. D. (1988) *J. Biol. Chem.* **263,** 15189–15195
23. Evans, D. H., and Linn, S. (1984) *J. Biol. Chem.* **259,** 10252–10259
24. Cantor, C. R., and Schimmel, P. R. (1980) *Biophysical Chemistry. Part I: The Conformation of Biological Macromolecules*, Freeman and Co., San Francisco, CA
25. Beaud, G., Beaud, R., and Leader, D. P. (1995) *J. Virol.* **69,** 1819–1826
26. Chrysogelos, S., and Griffith, J. (1982) *Proc. Natl. Acad. Sci. U. S. A.* **79,** 5803–5807
27. Griffith, J. D., Harris, L. D., and Register, J. (1984) *Cold Spring Harbor Symp. Quant. Biol.* **49,** 553–559
28. Alani, E., Thresher, R., Griffith, J. D., and Kolodner, R. D. (1992) *J. Mol. Biol.* **227,** 54–71
29. Bujalowski, W., Overman, L. B., and Lohman, T. M. (1988) *J. Biol. Chem.* **263,** 4629–4640
30. Bochkarev, A., Pfuetzner, R. A., Edwards, A. M., and Frappier, L. (1997) *Nature* **385,** 176–181
31. Lohman, T. M., and Ferrari, M. E. (1994) *Annu. Rev. Biochem.* **63,** 527–570